

An Optomechanical Pressure Sensor Using Multimode Interference Couplers

Dooyoung HAH*, Euisik YOON and Songcheol HONG

Department of Electrical Engineering, Korea Advanced Institute of Science and Technology,
 373-1 Kusong-dong, Yusong-gu, Taejeon, 305-338, Korea

(Received October 1, 1998; accepted for publication December 18, 1998)

A new optomechanical pressure sensor using multimode interference (MMI) couplers and a thin p⁺-Si membrane is presented. We simulate the device characteristics by the normal mode theory considering deflection and strain of the membrane. The optical waveguide is made of a single-mode, strip-loaded SiO₂-SiN_x-SiO₂ system. Device size can be reduced to 0.5 × 13 mm² by using a MMI coupler, and the total thickness of the membrane is 5.9 μm. The measured sensitivity is 11.98 ppm/Pa in a range of 50 kPa, which is larger than that of conventional capacitive sensors.

KEYWORDS: optomechanical pressure sensor, multimode interference couplers, p⁺-Si membrane, strip-loaded silica waveguide, photoelastic effect

1. Introduction

Semiconductor mechanical sensors have drawn considerable attention due to their likely advantages of small volume, batch fabrication and easy integration with electronic circuits. A silicon substrate is always considered a good candidate for use in these sensors due to its excellent electrical and mechanical properties. Most of reported semiconductor pressure sensors used the capacitive¹⁾ or piezoresistive²⁾ mechanisms. Capacitive sensors have shown good performance in terms of sensitivity, and piezoresistive sensors have shown good linearity. However, since both of them are fatally sensitive to electromagnetic radiation, optomechanical pressure sensors recent are a good alternative, especially in electromagnetically active environments. There are several reports on optomechanical pressure sensors.³⁻⁹⁾ Brabander *et al.* utilized an integrated-optical ring resonator which measures strain by frequency change, hence it needs additional circuits for encoding.³⁾ Kim and Neikirk measured pressure by the reflectance change of the Fabry-Perot cavity, the thickness control of which is very critical and complicated.⁴⁾ In refs. 5–9, Mach-Zehnder interferometers (MZIs) with Y-branches which are long (>1 cm) and have large loss were used. Also, bulk silicon membranes (≥60 μm) were used;^{5-7,9)} their thickness is difficult to control due to the absence of etch-stop layers. Therefore, their size must be large, at least 40 mm², for sufficient sensitivity. In this paper, we propose a new optomechanical pressure sensor using MMI couplers, which provide lower loss and are shorter than MZI. This new sensor also includes a thin p⁺-Si membrane which works as a etch-stop layer in order to reduce device size.

The schematic diagram of the proposed sensor is depicted in Fig. 1. It consists of two MMI couplers, two arms and a membrane. One arm (arm 1) is located on the membrane. MMI couplers can be designed to divide input light into two equal-power output lights.¹⁰⁾ When no pressure is applied to the membrane (Fig. 2(a)), the divided lights meet at the output MMI coupler in the same phase, so that they can be combined in the output MMI coupler. When some pressure is applied to the membrane (Fig. 2(b)), strain, due to deflection, is induced in the membrane, so that the phases of the two arms differ by the following two mechanisms. One is path lengthening, and the other is the photoelastic effect, which can be written as¹¹⁾

$$\Delta \left(\frac{1}{n_y^2} \right) = p_{yy} S_y + p_{yz} S_z, \quad (1)$$

where n_y is refractive index, p_{yy} , p_{yz} are photoelastic coefficients and S_y , S_z are strain. Hence, output power of an output MMI coupler is varied by pressure change.

2. Design and Simulation

2.1 Optical design

The waveguide layers are designed by a single-mode, strip-loaded SiO₂-SiN_x-SiO₂ system (Fig. 3), which is expected to have low loss. The thickness of the SiN_x core layer is 0.3 μm for single-mode operation at $\lambda = 632.8$ nm. The width and height of the strip are 5 μm and 0.2 μm, respectively. The thickness of the SiO₂ lower cladding layer is 1.5 μm to pre-

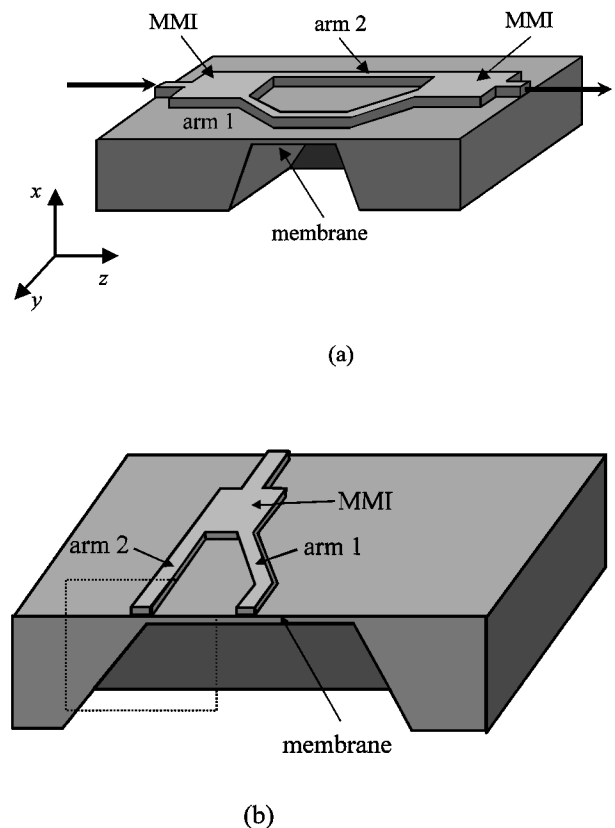


Fig. 1. Schematic cross section of the proposed sensor viewed in (a) the y direction and (b) the z direction.

*E-mail address: hady@oerc.kaist.ac.kr

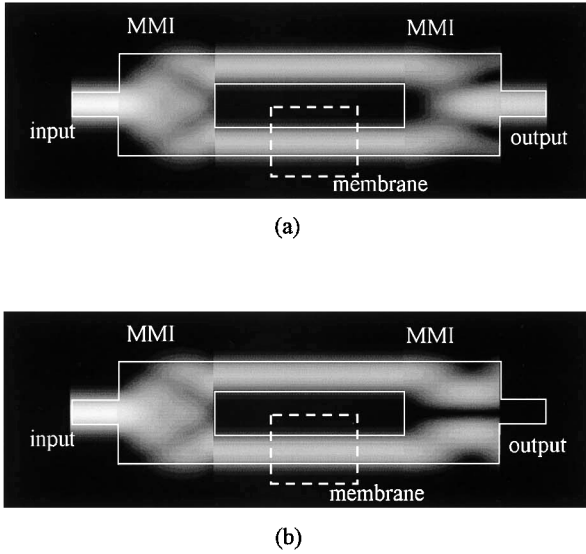


Fig. 2. Simulated light propagation mechanism of the proposed sensor when (a) no pressure is applied and (b) pressure is applied.

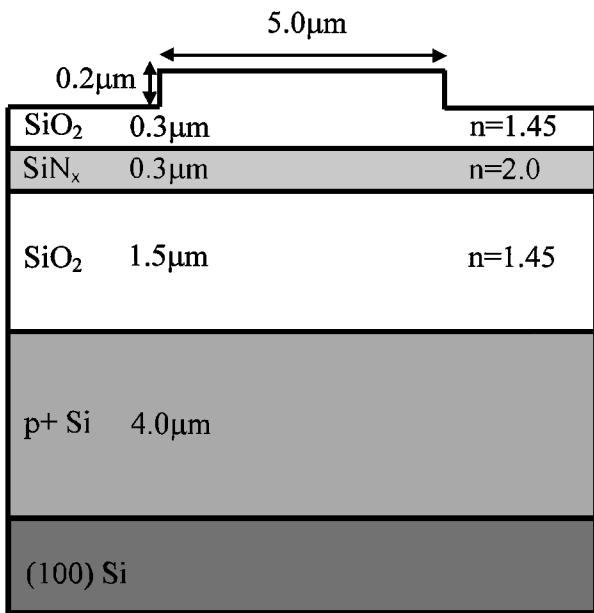


Fig. 3. Designed waveguide layer system.

vent light leakage to the Si substrate. The refractive index of each layer as measured by an ellipsometer is given in Fig. 3. The 3 dB dividing length of an MMI coupler, L_{3dB} , is expressed as (Fig. 4)¹⁰⁾

$$L_{3dB} \cong \frac{3p}{8} \frac{\pi}{\beta_0 - \beta_1} \cong \frac{p}{2} \frac{n_f}{\lambda_0} \left(W_M + \frac{\lambda_0}{\pi} \frac{1}{\sqrt{n_f^2 - n_s^2}} \right)^2, \quad (2)$$

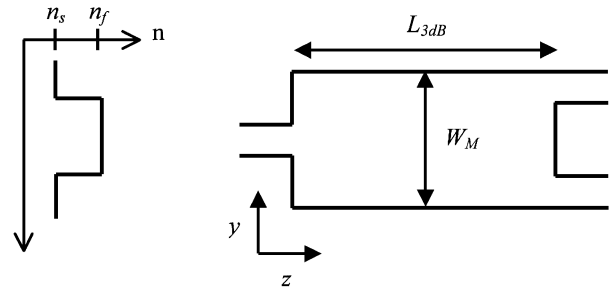


Fig. 4. Schematic diagram of MMI coupler.

where λ_0 is wavelength and p is an odd number. We must consider two facts in the design of MMI couplers. Those are that L_{3dB} increases as the width of the MMI coupler increases and the spacing between the two arms must be sufficient so that the lights propagating through the arms do not couple to each other. The designed width and L_{3dB} of MMI couplers are $20 \mu\text{m}$ and 3 mm , respectively, and the width and the length of arms are $5 \mu\text{m}$ and 7 mm , respectively. Therefore, the total length of the device is 13 mm , which is much smaller than that of the reported sensors using MZI ($>4 \text{ cm}$).

2.2 Mechanical design

Since dielectric thin films generally have large residual stress, they need a supporting layer to avoid initial deflection or buckling to form a membrane with the films. We also chose a p^+ -Si layer as the supporting layer. It is well known that a heavily boron-doped ($>7 \times 10^{19} \text{ cm}^{-3}$) Si layer has a large etching selectivity to bulk Si in an anisotropic Si etchant (ethylenediamine pyrocatechol, EDP), thus we can obtain a thin membrane with a well-controlled thickness by using this layer. The thickness is $4 \mu\text{m}$ with a mild tensile stress and the area is as small as 0.25 mm^2 .

2.3 Simulation

This simulation was performed via the following two steps. Firstly, the deflection and strain of the membrane due to pressure are calculated by an analytical method. Then, light propagation through the entire device is simulated by the normal mode theory (NMT)¹²⁾ and the mode propagation method (MPM)¹⁰⁾ with the strain calculated in the previous step. With NMT, we can obtain propagation constants and guided mode profiles of a given layer structure. At the interface between two different waveguide structures, the mode conversion factor is calculated by the overlap integral of the mode profiles of the two structures with MPM. If we assume that all membrane edges are built in, the deflection (w) is described by the superposition of the deflection of the simply supported plate (w_0) and that of the plate by moments distributed along the edges ($w_{1,2}$):¹³⁾

$$w = w_0 + w_1 + w_2 \quad (3a)$$

$$w_0 = \frac{4qa^4}{\pi^2 D} \sum_{m=1,3,5,\dots}^{\infty} \frac{(-1)^{(m-1)/2}}{m^5} \cos \frac{m\pi y}{a} \left(1 - \frac{\alpha_m \tanh \alpha_m + 2}{2 \cosh \alpha_m} \cosh \frac{m\pi z}{a} + \frac{1}{2 \cosh \alpha_m} \frac{m\pi z}{a} \sinh \frac{m\pi z}{a} \right) \quad (3b)$$

$$w_1 = -\frac{a^2}{2\pi^2 D} \sum_{m=1,3,5,\dots}^{\infty} E_m \frac{(-1)^{(m-1)/2}}{m^2 \cosh \alpha_m} \cos \frac{m\pi y}{a} \left(\frac{m\pi z}{a} \sinh \frac{m\pi z}{a} - \alpha_m \tanh \alpha_m \cosh \frac{m\pi z}{a} \right) \quad (3c)$$

$$w_2 = -\frac{b^2}{2\pi^2 D} \sum_{m=1,3,5,\dots}^{\infty} F_m \frac{(-1)^{(m-1)/2}}{m^2 \cosh \beta_m} \cos \frac{m\pi z}{b} \left(\frac{m\pi y}{b} \sinh \frac{m\pi y}{b} - \beta_m \tanh \beta_m \cosh \frac{m\pi y}{b} \right) \quad (3d)$$

$$D = \frac{Eh^3}{12(1-\nu^2)}, \alpha_m = \frac{m\pi b}{2a}, \beta_m = \frac{m\pi a}{2b},$$

where h , E , and ν are the thickness, Young's modulus, and Poisson's ratio of membrane, respectively, and E_m and F_m are calculated by boundary conditions. The maximum strain $(S_{y,z})_{\max}$ is expressed as

$$(S_y)_{\max} = -\frac{h\partial^2 w}{2\partial y^2}, \quad (S_z)_{\max} = -\frac{h\partial^2 w}{2\partial z^2} \quad (4)$$

Figure 5(a) is the calculated deflection profile and Figs. 5(b) and 5(c) are the calculated strain profiles along the z direction when pressure is applied to the membrane. Although the y component of strain (S_y) is largest at the edge ($y = a/2$) in the y direction, the deflection and the z component of strain (S_z) are largest at the center ($y = 0$) in the y direction. Hence, the phase change of an arm on the center (arm 1) is expected to be larger than that of an arm on the edge (arm 2). The light propagation through the device is drawn in Fig. 2, and the parameters used in this simulation are shown in Table I.

3. Fabrication

The sensor fabrication process is shown in Fig. 6; it starts with boron diffusion for 7 h at 1100°C to the (100) Si substrate in order to form a p^+ -Si etch-stop layer (a). The SiO_2 lower cladding layer is made by wet thermal oxidation for 1 h at 1000°C (0.3 μm) and sputtering deposition for 12 h (1.2 μm). Because thermal oxide has much larger residual stress than sputtered SiO_2 , the formation of the lower cladding layer is separated into two steps. Backside SiO_2 layer formed in this thermal oxidation process is used as a mask for bulk Si etching. The SiN_x core layer is deposited by remote plasma chemical vapor deposition for 28 min at 250°C. The SiO_2 upper cladding layer is deposited by sputtering for 3 h (b). Cr is deposited by e-beam evaporation and patterned by the lift-off process to form an etching mask layer for reactive ion beam etching (RIBE). The strip is formed by a combination of dry etching in RIBE with a mixture of CF_4 and Ar gas for 8 min, and wet etching in buffered oxide etchant (BOE) for 10 s (c). A front-back aligner is used for alignment of the waveguides and the membrane. After opening the window of the backside SiO_2 in BOE, anisotropic etching of bulk Si in EDP is performed for 8.5 h at 110°C for the membrane formation and the etching is stopped at the p^+ -Si layer. The composition of EDP used is ED:P:water=350 ml:115 g:115 ml (F-type), and the etch rate is about 1 $\mu\text{m}/\text{min}$ at that temperature. Finally, Cr is removed (d). Figure 7 shows the scanning electron micrograph of the fabricated device. The image corresponds to the inside of dotted box in Fig. 1(b). Actually, arm 2 is located on the inner edge of the membrane in the fabricated device. It is caused by the wafer-to-wafer thickness variation, and is not thought to deteriorate the device performance. Total thickness of the membrane is 5.9 μm . The root-mean-square roughness of p^+ -Si surface is about 10 nm (measured by an atomic force

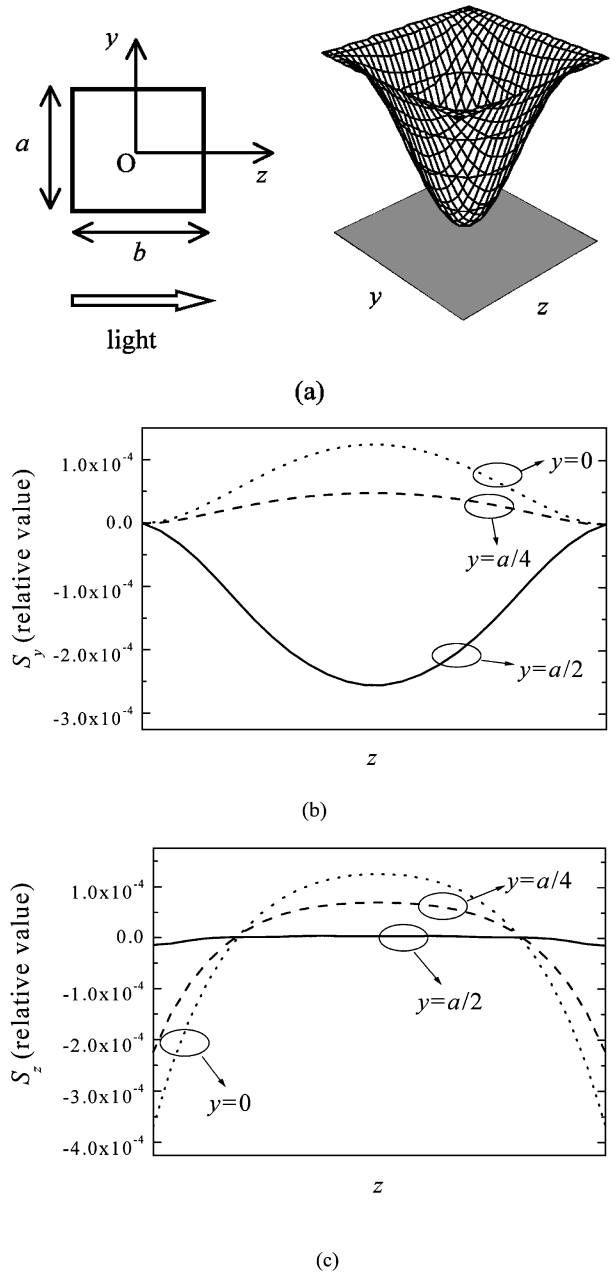


Fig. 5. Calculated profiles of (a) deflection, (b) strain of y component and (c) strain of z component of a membrane when pressure is applied.

Table I. parameter values used in simulation.

Young's modulus	E_{Si}	190 GPa
	E_{SiO_2}	90 GPa
	E_{SiN_x}	130 GPa
photoelastic coefficient	P_{yy}	0.121
	P_{yz}	0.270

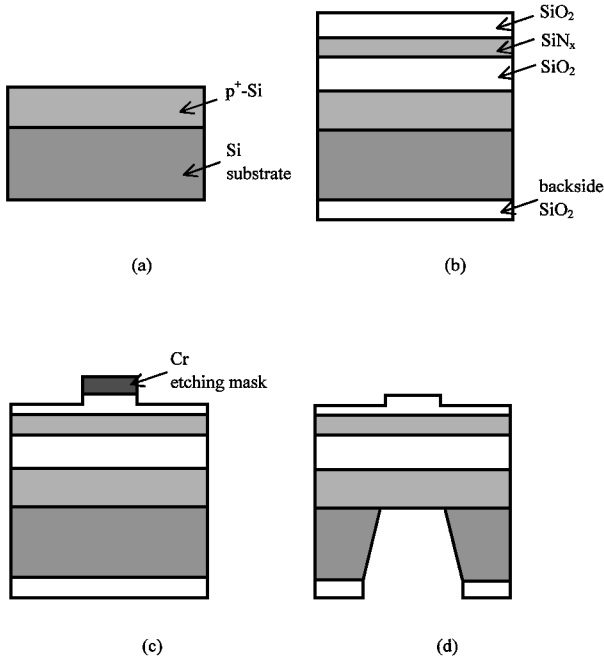


Fig. 6. Fabrication process of the proposed sensor.

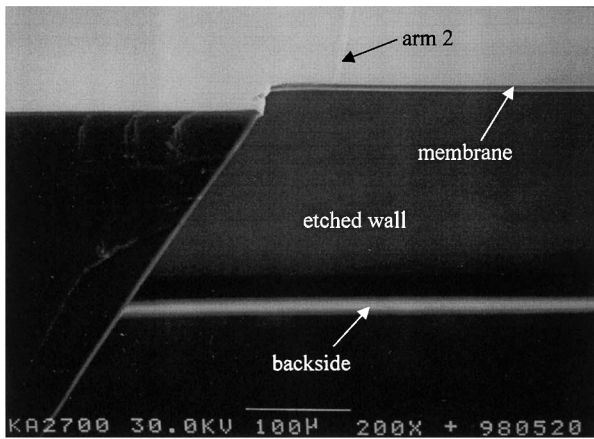


Fig. 7. Scanning electron micrograph of the fabricated sensor.

microscope), which corresponds to about 1/60 of the wavelength of the He-Ne laser. This is not thought to affect the optical performance significantly.

4. Results

Simulated characteristics of the proposed sensors with various membrane sizes are shown on Fig. 8. The simulated sensitivities of the sensor with the $0.5 \times 0.5 \text{ mm}^2$ and $0.4 \times 0.4 \text{ mm}^2$ membrane are 20.0 ppm/Pa in a range of 50 kPa and 8.22 ppm/Pa in a range of 100 kPa, respectively. There is almost no response in the $0.2 \times 0.2 \text{ mm}^2$ membrane case in a range of 100 kPa. A He-Ne laser ($\lambda = 632.8 \text{ nm}$) is used as the light source, and light is injected to the sensor via an objective lens. The measured characteristics of the fabricated sensor are shown with the simulated one in Fig. 9. Measured sensitivity is 11.98 ppm/Pa in a range of 50 kPa, which is higher than those of capacitive pressure sensors (typically $\sim 1 \text{ ppm/Pa}$). The difference between the measured and sim-

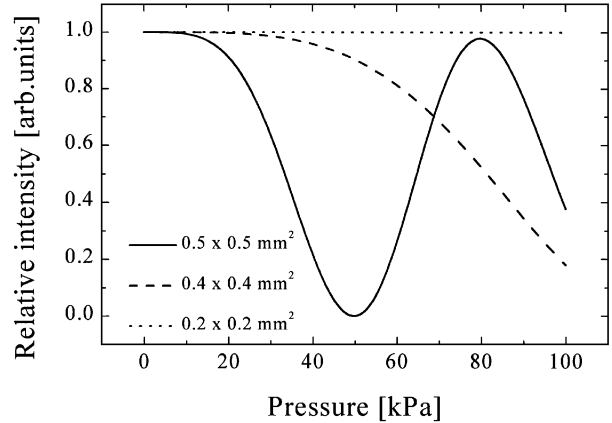


Fig. 8. Simulated characteristics of proposed sensors whose membrane sizes are $0.5 \times 0.5 \text{ mm}^2$ (solid line), $0.4 \times 0.4 \text{ mm}^2$ (dashed line), and $0.2 \times 0.2 \text{ mm}^2$ (dotted line).

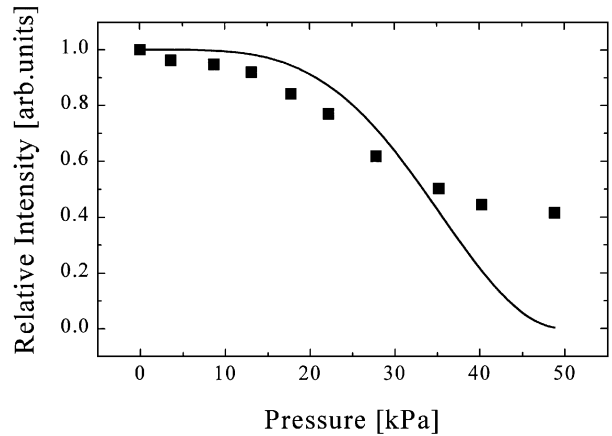


Fig. 9. Measured (squares) and simulated (solid line) characteristics of the proposed sensor.

ulated results may be caused by the difference between simulation and real device parameters.

5. Conclusions

An optomechanical pressure sensor using MMI couplers with $4\text{-}\mu\text{m}$ -thick $p^+\text{-Si}$ membrane is fabricated. The area of the sensor is considerably reduced to $0.5 \times 13 \text{ mm}^2$, which is smaller than that of previous optomechanical pressure sensors. The device characteristics are measured and compared with simulation results. The measured sensitivity is 11.98 ppm/Pa in a range of 50 kPa.

Acknowledgements

This work is partially supported by the Ministry of Information and Communication, and by the Korea Science and Engineering Foundation, OERC-1997G0202. The authors would like to thank Sookun Jeon, Euncheol Park, and Jinsung Park for aid in fabrication.

- 1) J. T. Kung and H. Lee: IEEE J. Microelectromech. Syst. **1** (1992) 121.
- 2) B. Folkmer, P. Steiner and W. Lang: Sensors & Actuators A **54** (1996) 488.
- 3) G. N. Brabander, J. T. Boyd and G. Beheim: IEEE Photon. Technol. Lett. **6** (1994) 671.

- 4) Y. Kim and D. P. Neikirk: IEEE Photon. Technol. Lett. **7** (1995) 1471.
- 5) D. Peters, K. Fischer and J. Muller: Sensors & Actuators A **25-27** (1991) 425.
- 6) C. Wagner, J. Frankenberger and D. P. Deimel: IEEE Photon. Technol. Lett. **5** (1993) 1257.
- 7) K. Fischer, J. Muller, R. Hoffmann, F. Wasse and D. Salle: J. Lightwave Technol. **12** (1994) 163.
- 8) K. Hoppe, L. U. A. Andersen and S. Bouwstra: Proc. 8th Int. Conf. Solid-state Sensors and Actuators, and Eurosensors IX, Stockholm, 1995, p. 590.
- 9) K. Benaissa and A. Nathan: IEEE Trans. Electron Devices **43** (1996) 1571.
- 10) L. B. Soldano and E. C. M. Pennings: J. Lightwave Technol. **13** (1995) 615.
- 11) A. Yariv and P. Yeh: *Optical Waves in Crystals* (John Wiley & Sons, New York, 1983) Chap. 9, p. 318.
- 12) H. Ribot, P. Sansonetti and A. Carenco: IEEE J. Quantum Electron. **26** (1990) 1930.
- 13) S. Timoshenko and S. Woinoswky-Krieger: *Theory of Plates and Shells* (McGraw-Hill, New York, 1959) 2nd ed., Chap. 6, p. 197.